aerospace

MDPI

Article

Real Time Measurement of Airplane Flutter via Distributed Acoustic Sensing

Ezzat G. Bakhoum [1,†,‡], Cheng Zhang [2,‡] and Marvin H. Cheng [3,*]

[1] Department of Electrical and Computer Engineering, University of West Florida, Pensacola, FL 32514, USA; ebakhoum@uwf.edu

[2] Department of Mechanical Engineering, University of West Florida, Pensacola, FL 32514, USA; czhang@uwf.edu

[3] Department of Mechanical and Aerospace Engineering, Embry Riddle Aeronautical University, Daytona Beach, FL 32114, USA

* Correspondence: CHENGM@erau.edu

† Current address: Department of Electrical and Computer Engineering, 11000 University Parkway, Pensacola, FL 32514, USA.

‡ These authors contributed equally to this work.

Received: 28 June 2020; Accepted: 25 August 2020; Published: 29 August 2020

Abstract: This research group has recently used the new technology Distributed Acoustic Sensing (DAS) for the monitoring and the measurement of airplane flutter. To the authors' knowledge, this is the first such use for this new technology. Traditionally, the measurement of airplane flutter requires the mounting of a very large number of sensors on the wing being monitored, and extensive wiring must be connected to all these sensors. The new system and technology introduced in this paper dramatically reduces the hardware requirements in such an application: all the traditional sensors and wiring are replaced with one fiber optic cable with a diameter of 2 mm. An electro-optical system with the size of a desktop PC monitors simultaneously one or more of such fiber optic cables and detects/characterizes any mechanical disturbances on the cables. Theoretical and experimental results are given.

Keywords: Distributed Acoustic Sensing; airplane flutter; Optical Time-Domain Reflectometry

1. Introduction

Flutter is a dangerous phenomenon that occurs when an airplane is moving at certain high speeds [1,2]. When flutter occurs, the wings and/or the control surfaces of the aircraft extract energy from the airflow and start vibrating, which can result in the disintegration of those structures. A central part of aircraft design, therefore, is the prediction of speeds at which flutter may occur. Usually, a computer model is developed, and then actual tests are performed on an airplane model in a wind tunnel and also on a full scale aircraft. Still, it is very desirable to include a mechanism to alert the pilot when an actual airplane in flight is about to experience flutter. Unfortunately, accurate measurement of flutter (that is, vibrations in the wings and/or the control surfaces) requires lots of sensors [3,4]. Even when the measurement of flutter in one wing is desired, very large numbers of accelerometers and strain gauges are usually required [4,5]. The hardware requirement is even made worse by the fact that wiring must be connected to all those sensors. For this reason, the actual measurement of flutter in production airplanes is impractical and hence not implemented by aircraft manufacturers at the present time.

It is the objective of this paper to introduce a novel new apparatus and method that takes real-time measurements of vibrations in production aircraft, operating under actual service conditions, with very

minimal hardware: just one fiber optic cable, with a diameter of 2 mm, that runs through each wing or control surface in the aircraft. Approximately one decade ago, a new technology known as Distributed Acoustic Sensing (DAS) was introduced [6] (the technology is based on foundational work reported earlier in [7,8]). A DAS system is essentially an optical system driven by a computer. The optical system, under computer control, sends pulses of laser light through a fiber optic cable. If the cable experiences even a slight bending at any location, laser light is scattered and is reflected back toward the source. The system, by making accurate measurements of the round-trip delay and other parameters, can determine precisely where the bending occurred and the magnitude of such bending. The technology became known as "Distributed Acoustic Sensing" because it is capable of detecting vibrations with frequencies within the acoustic range (generally, 0–20 kHz). The technique can detect such vibrations, and take measurements, at thousands of points simultaneously along the fiber optic cable. At the present time, DAS is used in applications such as the monitoring of the integrity of a pipeline and perimeter monitoring (to detect intrusions). To the best of the authors' knowledge, DAS has not yet been used in the application of flutter measurement. In this application, DAS will be a very attractive technology because all the hardware that is required to be installed inside a wing or a control surface is just one fiber optic cable, with an overall diameter of 2 mm. No other sensors, wiring, or hardware is required. In this paper, it is suggested that four such cables be used: one for each wing and one for each horizontal stabilizer. Figure 1 shows this concept and system.

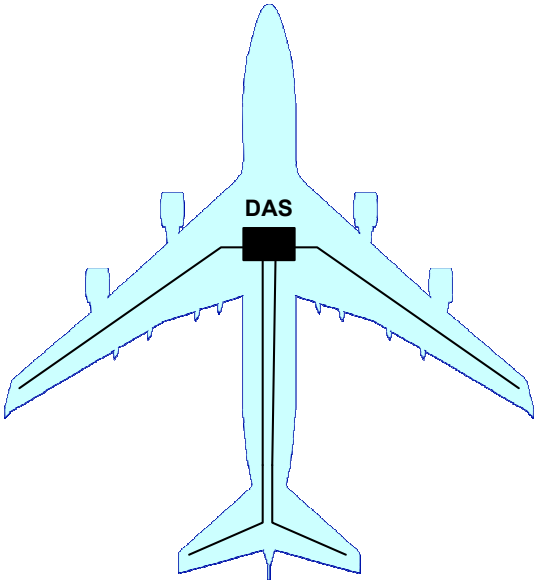

Figure 1. DAS system driving four fiber optic cables.

As Figure 1 also shows, the electro-optical system (DAS system) is carried inside the main body of the aircraft. The DAS system is contained in a box of about the size of a conventional desktop PC. The DAS system drives the 4 fiber optic cables as shown in the figure.

2. Qualitative Description of the DAS System

A block diagram of the DAS system that was built by the authors is shown in Figure 2. Figure 3 shows a photograph of the actual system. The system was assembled from components that are available commercially from certain companies (see Appendix A for details and model numbers).

A DAS system is based on the observation of a Rayleigh backscattered optical signal in the time domain, a principle known as Optical Time-Domain Reflectometry (OTDR) [9–18]. There are a number of variations in this technique, and Figure 2 shows what is known as a Coherent OTDR system. As shown in the figure, a continuous-wave narrowband laser source (wavelength = 1550 nm) is connected to an optical isolator, and then to a directional coupler. The coupler routes the beam,

with frequency ω_0, to an Acousto-Optic Modulator (AOM), while also routing some of the energy to a balanced receiver. The AOM is a laser-intensity modulator that is driven by an acoustic source; here, the pulse train shown in the figure. Hence, pulses of laser light (infrared) appear at the output of the AOM. However, the AOM has another property: it shifts the frequency of the light by a small frequency change $\Delta\omega$. This frequency-shifted light then flows through an Erbium-Doped Fiber Amplifier (EDFA), a circulator, and then finally to the fiber under test. A Rayleigh backscattered signal from the fiber, with a frequency of $\omega_0 + \Delta\omega$, is then subsequently combined with the native laser light in the balanced receiver, as shown. The balanced receiver takes the mathematical product of the two incoming signals (both at infrared frequencies in the present application), and this product is immediately routed to a band-pass filter (BPF) that selects only the frequency component $\Delta\omega$. The combination of the balanced receiver and the BPF is therefore a super-heterodyning process, where the emerging low frequency $\Delta\omega$ is an intermediary frequency (IF). To recover the pulse stream (now delayed in time after traveling through the fiber under test), the IF is then routed to an envelope detector. The returning pulse stream is finally analyzed in the data acquisition module. It is to be noted that the data acquisition module is also responsible for generating the original pulse stream, as shown in the figure. Hence by analyzing the differences between the original and the secondary pulse streams, the data acquisition module (which feeds to a computer for data processing) can determine the round-trip delay and other parameters, such as the number of Rayleigh backscattered signals and the magnitudes of such signals.

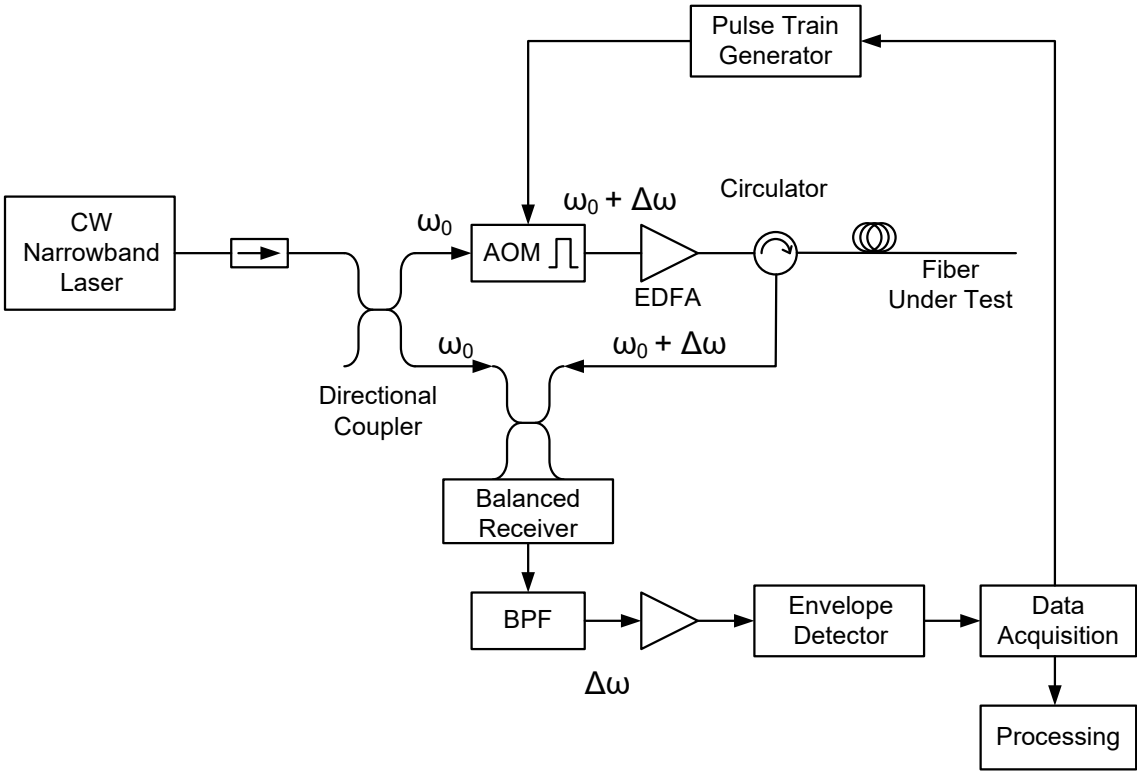

Figure 2. Block diagram of the DAS system used in the present application.

Figure 3. Photograph of the DAS system. This system drives four fiber optic cables.

At any point in time, there should be only one pulse propagating on the fiber in order to avoid crosstalk. By knowing the length of the fiber and the speed of propagation of light in glass (approximately 2×10^8 m/s), the maximum pulse rate can be determined. For example, for a 1 km—long fiber, the round-trip delay of a pulse is 10 μs, and hence the maximum pulse rate will be 100 kHz. This pulse rate is also the sampling rate of the DAS system (i.e., one pulse corresponds to one sample. Note that the sampling rate can be higher if a shorter fiber is used). With this sampling rate, and in order to satisfy the Nyquist criterion, events with frequencies up to 50 kHz can be reliably detected and measured with the present DAS system. This performance is more than adequate for the present application, since flutter frequencies are practically much less than 50 kHz. Another parameter that must be determined is the spatial resolution of the DAS system (that is, the minimum physical distance between two detectable events). In the present application, a spatial resolution of 10 cm was chosen. This indicates that the pulse duration should be approximately 0.5 ns (or 500 ps). Figure 4 shows the properties of the pulse train used in the present application.

Figure 4. Pulse train used in the present DAS system (frequency = 1 to 100 kHz; pulse duration = 0.5 ns).

3. Theoretical Background

3.1. Rayleigh Backscattering in a Multimode Optical Fiber

A theory will be now presented in which the phase difference between the incident and the reflected pulses is used as the basis for determining the location of bending along the fiber, and where the power of the Rayleigh backscattered pulse is used for determining the magnitude of the bending.

For light propagation in a glass fiber (a lossy dielectric medium), the energy W as a function of distance is given by the familiar equation [6,19]

$$W = W_0\, e^{-\alpha x} \tag{1}$$

where W_0 is the original (unattenuated) energy, x is distance, and α is an attenuation constant in nepers/m. (Note that α is not necessarily the same as the attenuation constant of the electric field intensity, because the energy/power in the propagating wave is actually proportional to the square of the electric field intensity [19]). The rate of change of energy with distance will be

$$\frac{dW}{dx} = -\alpha\, W_0 e^{-\alpha x} \tag{2}$$

For a pulse of light that is spread over a distance Δx, the energy contained in the pulse will be given by

$$W_{pulse} = \alpha\, W_0 e^{-\alpha x}\, \Delta x \tag{3}$$

Let us assume that a bending in the fiber occurs at a distance l from the source. The Rayleigh scattered pulse will arrive back at the source at a time $t = 2l/c$, where $c \approx 2 \times 10^8$ m/s is the speed of propagation in glass. Upon its arrival, the pulse will have an energy

$$W_{pulse} = \alpha\, R\, W_0 e^{-2\alpha l}\, \Delta x, \tag{4}$$

where R is the fraction of the light that travels backwards toward the source. The duration of the pulse will be equal to $\Delta x/c$; hence, by dividing Equation (4) by that duration, we obtain the power P of the received pulse:

$$\begin{aligned} P &= \alpha\, c\, R\, W_0 e^{-2\alpha l} \\ &= \alpha\, c\, R\, W_0 e^{-2\alpha (ct/2)} \\ &= P_0\, T\, \alpha\, c\, R\, e^{-\alpha c t} \end{aligned} \tag{5}$$

where W_0 has been replaced by $P_0 T$, where P_0 is the original (unattenuated) power of the pulse and T is the pulse duration. The Rayleigh scattered and captured fraction, R, is given by [7,8]

$$R = \frac{(NA)^2}{4n^2} \tag{6}$$

for a graded-index fiber (the type of fiber used in the present system), where NA is the numerical aperture of the fiber [6] and n is the index of refraction along the axis of the fiber. When the backscattered power is measured as a function of time, any anomaly in the normal Rayleigh backscattering (that is, deviation from Equation (5)) is typically caused by effects such as bending or local defects in the fiber. Figure 5 shows a typical plot of the backscattered power as a function of time, where an original pulse and a reflected pulse are shown. A bending in the fiber, for instance, at a distance l from the source, results in the reflected pulse shown in the figure, where the time lag between the original and the reflected pulses is $t = 2l/c$. From the time lag measurement, the distance l can be determined. Furthermore, the intensity of the reflected pulse is a function of the amount of bending in the fiber (see the experimental section below).

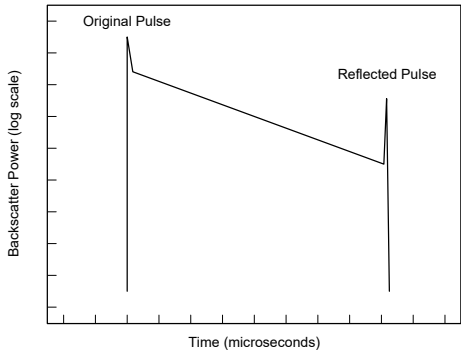

Figure 5. Typical plot of the backscattered power as a function of time.

3.2. Flutter and the Aeroelasticity Equation

Mechanically, flutter is described by the so-called aeroelasticity equation for wings [1]. This is usually an equation of the form

$$\mathrm{A}\ddot{\vec{q}} + (\rho V \mathrm{B} + \mathrm{D})\,\dot{\vec{q}} + \left(\rho V^2 \mathrm{C} + \mathrm{E}\right)\vec{q} = 0 \tag{7}$$

which, fully expanded, takes the form

$$
\begin{aligned}
m\begin{pmatrix} \frac{cs^5}{5} & \frac{s^4}{4}\left(\frac{c^2}{2}-cx_f\right) \\ \frac{s^4}{4}\left(\frac{c^2}{2}-cx_f\right) & \frac{s^3}{3}\left(\frac{c^3}{3}-c^2x_f+cx_f^2\right) \end{pmatrix}\begin{pmatrix} \ddot{q}_1 \\ \ddot{q}_2 \end{pmatrix} \\
+\rho V\begin{pmatrix} \frac{ca_ws^5}{10} & 0 \\ -\frac{c^2ea_ws^4}{8} & -\frac{c^3s^3M_{\dot{\theta}}}{24} \end{pmatrix}\begin{pmatrix} \dot{q}_1 \\ \dot{q}_2 \end{pmatrix} \\
\left(\rho V^2\begin{pmatrix} 0 & \frac{ca_ws^4}{8} \\ 0 & -\frac{c^2ea_ws^3}{6} \end{pmatrix}+\begin{pmatrix} 4EIs & 0 \\ 0 & GJs \end{pmatrix}\right)\begin{pmatrix} q_1 \\ q_2 \end{pmatrix} \\
=\begin{pmatrix} 0 \\ 0 \end{pmatrix}
\end{aligned}
$$

where

- q_1 and q_2 are the generalized coordinates κ (flap) and θ (pitch angle);
- ρ is the air density;
- V is the true airspeed;
- m is the mass per unit area of the wing;
- c is the chord length;
- s is the span;
- e is the distance from the flexural axis to the lift center divided by the chord length;
- x_f is the distance from the leading edge of the wing to the flexural axis;
- a_w is the slope of the lift curve;
- $M_{\dot{\theta}}$ is the derivative of the angular moment around the flexural axis;
- EI is the bending rigidity;
- GJ is flexural (or torsional) rigidity.

Unfortunately, for most modern airfoils it is very difficult to determine all the parameters in the equation precisely, and hence the numerical models are usually unreliable. (Please note that Equation (7) is given here for reference only, and no attempt is made in this paper to solve the equation. This paper is concerned only with the practical, real-time measurement of flutter.) For this reason, aircraft manufacturers usually rely on experimentation (in wind tunnels and on full scale aircraft) to determine the flutter parameters of a wing, such as bending (flap) and torsion as a function of speed and altitude. The DAS system introduced here makes the experimental determination of the flutter parameters quite easy, and, as described above, can also be used for the real-time monitoring of vibrational disturbances in aircraft under actual operating conditions.

4. Experimental Results

4.1. The Experimental Setup

A large model airplane was tested in a wind tunnel. The model is a 1/26-scale of a Boeing 747 (made by Giant RC Co., Hong Kong, China). The wingspan of the model measures 248 cm and the length measures 272 cm. The wind tunnel that was used is a NASA facility (at the Langley research center). The tunnel provides wind speeds of up 1000 km/h (620 mi/h). Figure 6 shows a photograph of the model airplane inside the wind tunnel.

Figure 6. Photograph of the model airplane inside the wind tunnel.

The model that was chosen is a radio controlled model that can be actually flown. It has wings that are made with steel and aluminum ribs and spars, and are covered with a fiberglass skin. Thus, the performance of the wings at high airspeeds should resemble closely the performance of the wings in a full scale aircraft. Regardless, the objective of the test was to determine the capability of the DAS system in monitoring mechanical disturbances in real time. Figure 7 shows a photograph of the back of the airplane inside the tunnel, with the airflow turned off.

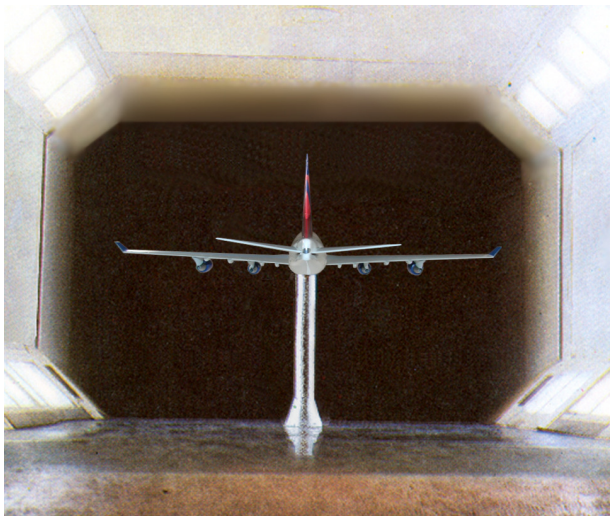

Figure 7. Photograph of the back of the airplane (airspeed = 0).

As shown in Figure 1, four fiber optic cables, each with a diameter of 2 mm [20], were inserted inside the wings and the horizontal stabilizers (the cables were attached to the main spars). The cables were then attached to the DAS system, as shown in Figure 3.

4.2. Flutter Measurements

The model was tested at different airspeeds, at a simulated altitude of 10,000 ft. It is possible, by varying the air density inside the tunnel, to perform the test at other simulated altitudes, and these results are summarized at the end of this section. The main objective of the test was to study the

performance of the DAS system, rather than to conduct full aerodynamic analysis of the model airplane. At the simulated altitude of 10,000 ft, flutter was observed to occur in the wings at two specific speeds: Mach number M = 0.63 and M = 0.75. At M = 0.63, only bending in the wing was observed, with a frequency of 5.1 Hz. At Mach number M = 0.75, a mode that combines both bending and torsion was observed, at a frequency of 7.8 Hz. (Fortunately, the model airplane did not break apart when the first flutter event occurred, but the wings suffered some permanent deformation). Table 1 summarizes these results.

Table 1. Flutter modes and their frequencies.

Mode	Frequency	Airspeed
Bending	5.1 Hz	M 0.63
Bending/Torsion	7.8 Hz	M 0.75

It must be pointed out that higher modes of flutter (with higher frequencies) likely exist, but discovering these modes require a supersonic tunnel for testing (a facility that was not available for the authors). Figure 8 shows flutter occurring at Mach number M = 0.63. The two photographs were taken 0.098 s apart.

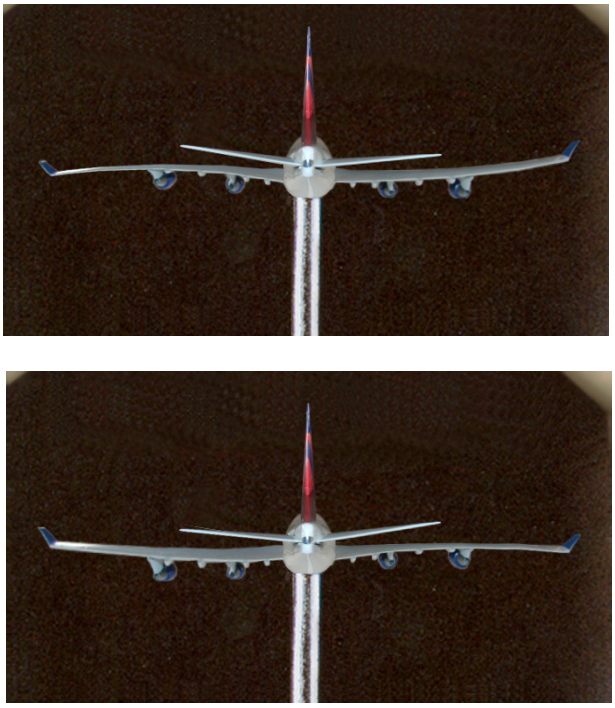

Figure 8. Flutter occurring at Mach 0.63. The two photographs were taken 0.098 s apart.

The DAS system generates real-time data in the form of intensity of reflected light, which is proportional to bending in the fiber optic cable, as a function of two parameters: distance and time. Figure 9 shows the pure bending mode that occurs at a frequency of 5.1 Hz. The figure shows that maximum bending occurs approximately in the mid-section of the wing, with a half-period of 98.5 ms (that is, a frequency of 5.1 Hz).

Figure 10 shows the bending/torsion mode that occurs at a frequency of 7.8 Hz. Torsion is evident from the "zig-zag" pattern that exists in each data array that corresponds to one particular instant of time.

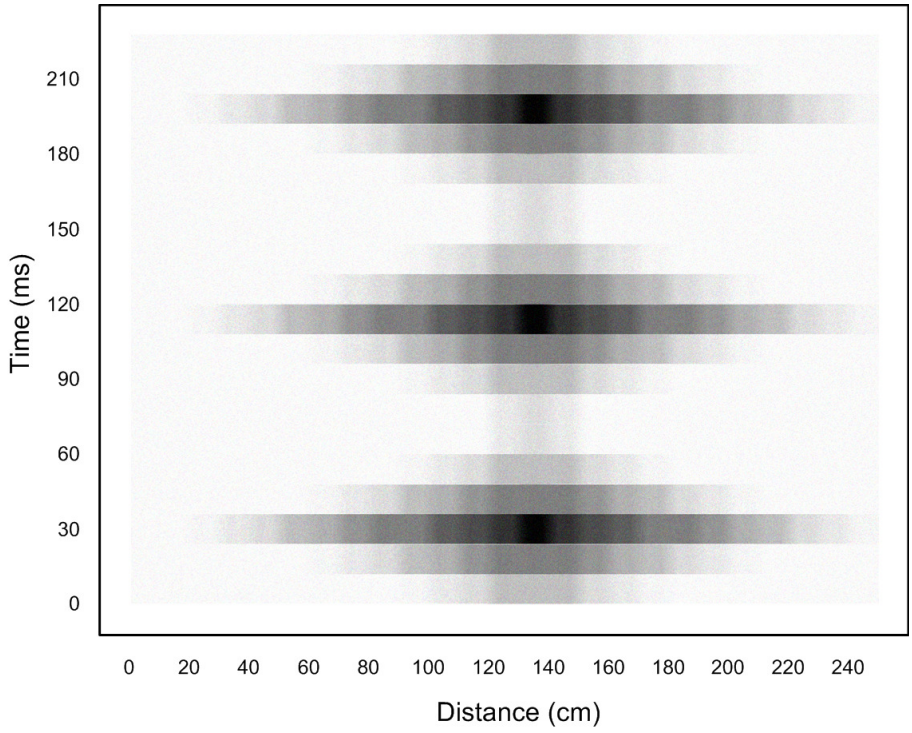

Figure 9. Time–distance data plot. Frequency = 5.1 Hz. (Shading represents intensity of reflected light).

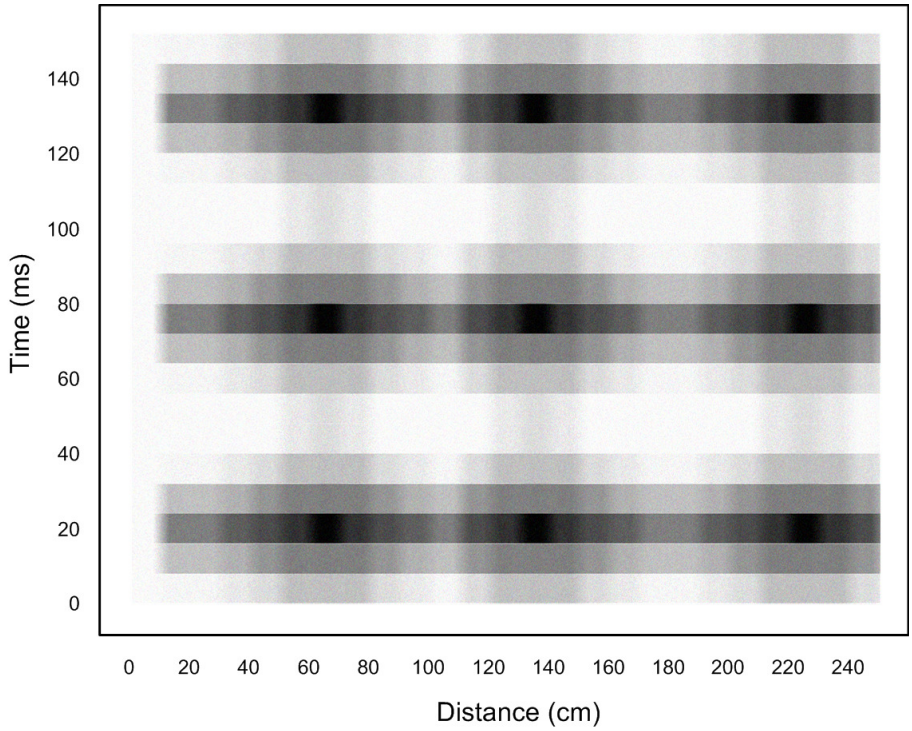

Figure 10. Time–distance data plot. Frequency = 7.8 Hz.

Concerning the intensity of the Rayleigh backscatter and the bending detected along the fiber, the following optical properties of the fiber were used in the calculations [20]:

- $NA = 0.22$;
- $n = 1.45$;
- $\alpha = 0.18$ dB/km, or approximately 4.14×10^{-5} nepers/m;
- $c \approx 2 \times 10^8$ (speed of light in glass fibers).

With a pulse duration of 0.5 ns, Equations (5) and (6) give

$$\frac{P}{P_0} = 2.38 \times 10^{-8}\, e^{-\alpha c t} \tag{8}$$

Pulses are detected as deviations from Equation (8) (see Figure 5; the stronger the pulse the stronger the deviation from the equation, and hence the stronger the bending in the cable). Figures 9 and 10 show the intensity of the detected pulses on an arbitrary scale (pulses appear as dark color; the Rayleigh backscatter appears as a gray background). It is evident that the bending vibrations have a sinusoidal pattern as a function of time.

4.3. Extended Tests

4.3.1. Tests at Different Altitudes

The wind tunnel that was used can control the density of the air (by injecting supercooled nitrogen into the air flow), and hence can simulate the actual atmosphere at various altitudes. Additional testing was done at simulated altitudes of 20,000 ft and 30,000 ft. As expected, the flutter frequencies were different from the frequencies given in Table 1; but otherwise the tests were unremarkable and the DAS system showed results that are very similar to the results shown above.

4.3.2. Damping as a Function of Airspeed

The damping of the two modes of flutter (bending and torsion) was theoretically analyzed with a frequency domain technique that is described in [21]. Figure 11 shows a plot of the damping factor for the two modes as a function of airspeed. It is evident that flutter occurs at airspeeds of M = 0.63 and M = 0.75 because the zero crossing occurs at those airspeeds. It is also evident that the bending mode becomes less stable at speeds above the flutter speed.

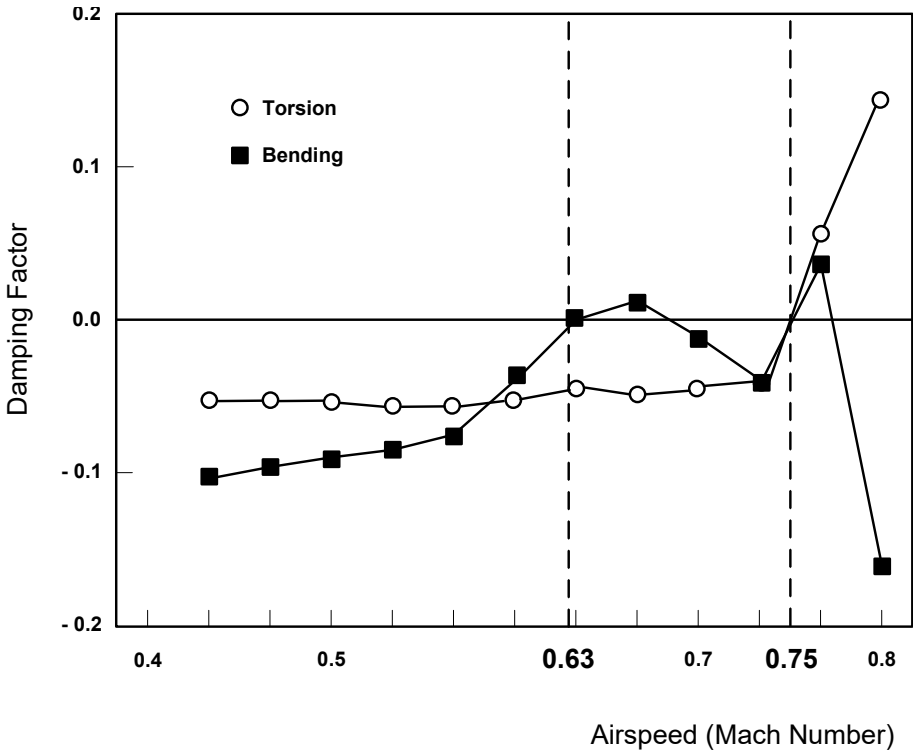

Figure 11. Calculated damping factor versus airspeed for the two modes of flutter.

4.3.3. Verification of Flutter Frequencies

The flutter tests were repeated with a traditional sensing method: a group of accelerometers and strain gauges that were attached to the surface of the wing (as shown in Figure 12). The accelerometers and strain gauges capture the bending and torsion strains that occur at various points on the wing. This method is simple and is described in references such as [4]. The flutter frequencies of 5.1 Hz and 7.8 Hz were confirmed.

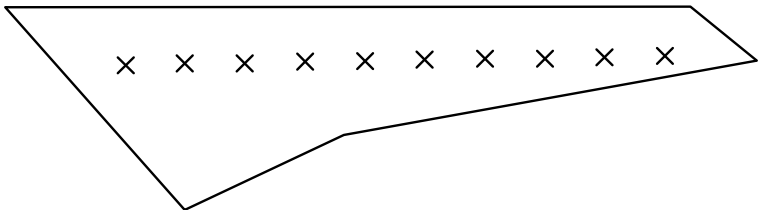

Figure 12. Locations of accelerometers and strain gauges on the surface of the wing.

5. Conclusions

The new method and apparatus for detecting and characterizing flutter described in this paper have very low hardware requirements, specifically, one fiber optic cable with an overall diameter of 2 mm to be inserted in each wing or control surface that must be monitored. The system can easily detect and characterize vibrations and torsion in these surfaces at the typical flutter frequencies or even at much higher frequencies. The system is useful not only for testing inside wind tunnels, but also for real time monitoring of flutter in full scale airplanes operating under actual service conditions.

Author Contributions: E.G.B.: Theoretical and experimental sections. C.Z.: Theoretical section. M.H.C.: Theoretical and experimental sections. All authors have read and agreed to the published version of the manuscript.

Funding: This research received no external funding. The APC was funded by the authors.

Conflicts of Interest: The authors declare no conflicts of interest.

Appendix A

List of optical components used in the DAS system:

Laser source: NKT PHOTONICS CORP., model number X15, wavelength: 1550 nm.

AOM: BRIMROSE CORP., model number TEM-250-50-5-2FP (custom modified to meet a rise time of 0.5 ns), wavelength: 380–1600 nm.

Balanced optical receiver: MKS NEWPORT Corp., model number Nirvana 1837, wavelength: 900–1650 nm.

References

1. Wright, J.R.; Cooper, J.E. *Introduction to Aircraft Aeroelasticity and Loads*; Wiley: New York, NY, USA, 2007.
2. Battoo, R.S. An introductory guide to literature in aeroelasticity. *Aeronaut. J.* **1999**, *103*, 511–518. [CrossRef]
3. Lind, R.; Brenner, M. *Robust Aeroservoelastic Stability Analysis*; Springer: London, UK, 1999.
4. Lind, R.; Brenner, M. The Flutterometer: An On-Line Tool to Predict Robust Flutter Margins. *J. Aircr.* **2000**, *37*, 1105–1112. [CrossRef]
5. Sydenham, P.H. Acceleration Measurement. In *Handbook of Measuring System Design*; Wiley: New York, NY, USA, 2005.
6. Hartog, A.H. An Introduction to Distributed Optical Fiber Sensors; CRC Press: Boca Raton, FL, USA, 2017.
7. Personick, S.D. Photon Probe—An Optical-Fiber Time Domain Reflectometer. *Bell Syst. Tech. J.* **1977**, *56*, 355–366. [CrossRef]
8. Neumann, E.G. Analysis of the backscattering method for testing optical fiber cables. *Arch. Elektr. Ubertragungstechnik (AEU)* **1980**, *34*, 157–160.

9. Daley, T.M.; Freifeld, B.M.; Franklin, J.A.; Dou, S.; Pevzner, R.; Shulakova, V.; Kashikar, S.; Miller, D.E.; Goetz, J.; Henninges, J.; et al. *Field Testing of Fiber-Optic Distributed Acoustic Sensing (DAS) for Subsurface Seismic Monitoring*; The Leading Edge; Society of Exploration Geophysicists: Tulsa, OK, USA, 2013; pp. 936–942.
10. Zhang, X.; Sun, Z.; Shan, Y.; Li, Y.; Wang, F.; Zeng, J.; Zhang, Y. A High Performance Distributed Optical Fiber Sensor Based on Φ-OTDR for Dynamic Strain Measurement. *IEEE Photonics J.* **2017**, *9*, 6802412. [CrossRef]
11. Muanenda, Y.; Oton, C.J.; Faralli, S.; Pasquale, F.D. A Cost-Effective Distributed Acoustic Sensor Using a Commercial Off-the-Shelf DFB Laser and Direct Detection Phase-OTDR. *IEEE Photonics J.* **2016**, *8*, 6800210. [CrossRef]
12. Martins, H.F.; Shi, K.; Thomsen, B.C.; Martin-Lopez, S.; Gonzalez-Herraez, M.; Savory, S.J. Real time dynamic strain monitoring of optical links using the backreflection of live PSK data. *Opt. Express* **2016**, *24*, 22303–22318. [CrossRef] [PubMed]
13. Reinsch, T.; Henninges, J.; Götz, J.; Jousset, P.; Bruhn, D.; Lüth, S. Distributed Acoustic Sensing Technology for Seismic Exploration in Magmatic Geothermal Areas. In Proceedings of the World Geothermal Congress 2015, Melbourne, Australia, 19–25 April 2015; pp. 1–5.
14. Dou, S.; Lindsey, N.; Wagner, A.M.; Daley, T.M.; Freifeld, B.; Robertson, M.; Peterson, J.; Ulrich, C.; Martin, E.R.; Ajo-Franklin, J.B. Distributed Acoustic Sensing for Seismic Monitoring of The Near Surface: A Traffic-Noise Interferometry Case Study. *Nat. Sci. Rep.* **2017**, *7*, 11620. [CrossRef] [PubMed]
15. Parker, T.; Shatalin, S.; Farhadiroushan, M. Distributed Acoustic Sensing—A new tool for seismic applications. *First Break* **2014**, *32*, 61–69. [CrossRef]
16. Bona, A.; Dean, T.; Correa, J.; Pevzner, R.; Tertyshnikov, K.V.; Zaanen, L.V. Amplitude and Phase Response of DAS Receivers. In Proceedings of the 79th EAGE Conference & Exhibition 2017, Paris, France, 12–15 June 2017; p. We A5 13.
17. Weng, Y.; Ip, E.; Pan, Z.; Wang, T. Advanced Spatial-Division Multiplexed Measurement Systems Propositions—From Telecommunication to Sensing Applications: A Review. *Sensors* **2016**, *16*, 1387. [CrossRef] [PubMed]
18. Lindsey, N.; Martin, E.R.; Dreger, D.S.; Freifeld, B.; Cole, S.; James, S.R.; Biondi, B.L.; Ajo-Franklin, J.B. Fiber-Optic Network Observations of Earthquake Wavefields. *Geophys. Res. Lett.* **2017**, *44*, 1–8. [CrossRef]
19. Hayt, W.H.; Buck, J.A. *Engineering Electromagnetics*; McGraw Hill: New York, NY, USA, 2006.
20. *Datasheet: Application Specific Optical Fibers for Sensors*; OFS Fitel: Norcross, GA, USA, 2017.
21. Follador, R.D.C.; Souza, C.E.D.; Marto, A.G.; Silva, R.G.A.D.; Góes, L.C.S. Comparison of In-Flight Measured and Computed Aeroelastic Damping: Modal Identification Procedures and Modeling Approaches. *J. Aerosp. Technol. Manag.* **2016**, *8*, 163–177. [CrossRef]